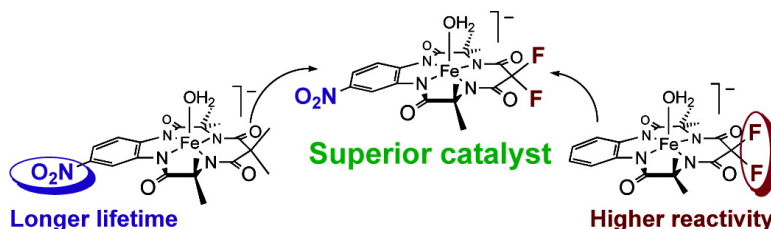Communication

Mechanistically Inspired Design of Fe#TAML Peroxide-Activating Catalysts

Delia-Laura Popescu, Arani Chanda, Matthew J. Stadler, Sujit Mondal,
Jacqui Tehranchi, Alexander D. Ryabov, and Terrence J. Collins

More About This Article

Additional resources and features associated with this article are available within the HTML version:

- Supporting Information
- Access to high resolution figures
- Links to articles and content related to this article
- Copyright permission to reproduce figures and/or text from this article

View the Full Text HTML

Mechanistically Inspired Design of Fe^{III}−TAML Peroxide-Activating Catalysts

Delia-Laura Popescu, Arani Chanda, Matthew J. Stadler, Sujit Mondal, Jacqui Tehranchi,
Alexander D. Ryabov,* and Terrence J. Collins*

Institute for Green Science, Carnegie Mellon University, 4400 Fifth Avenue, Pittsburgh, Pennsylvania 15213

Received July 2, 2008; E-mail: tc1u@andrew.cmu.edu; ryabov@andrew.cmu.edu

Iterative ligand design to optimize environmental compatibility and technical performance has come to define the field of green homogeneous oxidation catalysis.[1,2] To date, qualitative concepts have guided the development of the signature catalysts, the family of Fe^{III}−TAML activators, **1**, which activate peroxides according to Scheme 1.[1,2] A growing body of mechanistic data[3−7] now link ligand structural features to differential reactivities for the diverse processes of Scheme 1. These include the relative Fe−TAML (i) hydrolytic and (ii) operational stabilities, as well as (iii) their comparative speeds of peroxide activation, and (iv) the pHs of highest activities. Here we show how *quantitative* knowledge of the i−iv rates for the known Fe^{III}−TAMLs (**1b**−**e**) has been used to inform the design of the new catalyst **1a** to attain superior catalytic activity. The often-conflicting challenges of optimizing performance with environmental and precautionary factors are considered for **1a** in the conclusion.

TAML structural units that regulate the interplay of i−iv have been discovered. First, Fe^{III}−TAMLs attain huge gains in hydrolytic stability when tail R = F replaces R = CH$_3$ (Scheme 1) with inhibition of H$^+$-induced demetalation (k_d-associated step) reaching 10 orders of magnitude.[3] Moreover, for R = F, buffer ion-induced demetalation is eliminated altogether (k_b-associated step).[7] Thus, the difluoromalonyl tail unit is an excellent hydrolysis quencher for performance optimized Fe^{III}−TAMLs.

Second, the rate of degradation of **1** under operating conditions (k_i-associated step) parallels the peroxidase-like activity (k_{II}-associated step), increasing significantly from the CH$_3$- to F-tailed species.[4] Thus, any gain in k_{II} is partially neutralized by the increased k_i. However, kinetics reveals[4] that electron-withdrawing aromatic head substituents slow the rate of oxidative decomposition (surprise) while speeding up substrate oxidation (anticipated); the slope of the log k_{II} versus log k_i plot $\approx$ −1. Thus, strongly electron-withdrawing head groups are valuable for both increasing the reactivity and extending the lifetime.

Third, the reactivity of the prototype Fe^{III}−TAML, **1b**, toward H$_2$O$_2$ (k_I-associated step) is highest around pH 10.[5,6] Fe^{III}−TAML**s** are octahedral diaqua species in water.[3] The pH dependence of the rate of peroxidase-like activity is controlled by the Fe^{III}−TAMLs' first pK_a values ($\sim$10) and by the H$_2$O$_2$ pK_a (>11). Among Fe^{III}−TAML species, singly deprotonated [FeL(OH)(H$_2$O)]$^{2-}$ reacts most rapidly with H$_2$O$_2$, but slower with HO$_2^-$. For applications in water, it would be preferable for the highest rate to occur close to pH 7. Strong electron-withdrawing groups on both the head and the tail TAML sections should lower the pK_a of **1** and this insight provides a tool for moving the fastest rate toward neutral pH.[3]

To summarize the mechanistically derived design thinking, the strong TAML donor capacities allow iron to access high valent reactive intermediates enabling exceptional peroxidase-like reactivities. However, kinetics reveals that the i−iv rates are variously increased or decreased to favor overall improved performance when this same donor capacity is attenuated by substituent perturbations.

Scheme 1. Fe^{III}−TAML Activators (**1**) Used Were Solid 5-Coordinate Monoaqua Li Salts: **1a**, X$_1$ = NO$_2$, X$_2$ = H, R = F; **1b**, X$_1$ = X$_2$ = H, R = Me; **1c**, X$_1$ = X$_2$ = H, R = F; **1d**, X$_1$ = X$_2$ = Cl, R = F; **1e**, X$_1$ = NO$_2$, X$_2$ = H, R = Me^a
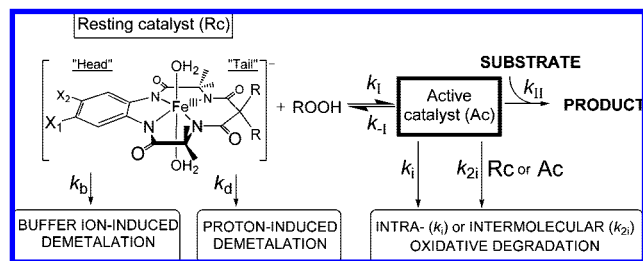

^{a} Major processes identified under operating conditions. Rate constants k_d and k_b describe proton- and buffer-induced demetalation of **1**, respectively;[3,7] k_i intra- and k_{2i} intermolecular inactivation, when Fe^{III}−TAML catalysis employs very low [**1**] (low nM), the k_{2i} pathway can be negligible.[4]

Therefore, an Fe^{III}−TAML with a tail CF$_2$ and an electron-withdrawing NO$_2$ headgroup, **1a**, prepared by standard techniques,[8] should outperform all existing members of its class giving the highest reactivity with its fastest rate closest to pH 7, the longest lifetime, and the highest turnover number.

Hydrolytic Stability (i). In contrast with **1b**, **1a** is immune to demetalation by the components of phosphate buffer at pH 5−7. It reacts more slowly with H$^+$ than **1c**; at [H$^+$] = 2.0 M and 25 °C, the pseudo-first-order rate constants for Fe^{3+} release measured here are (2.56 ± 0.03) × 10^{-4} for **1a** and (10.6 ± 0.5) × 10^{-4} s^{-1} for **1c**. Thus, the NO$_2$ headgroup delivers a >4-fold stability gain.

Operational Stability (ii). UV−vis traces of the **1a**-catalyzed *incomplete* bleaching of Safranine O by H$_2$O$_2$ (Supporting Information, Figure 1S) were fitted as in our previous study[4] using the equation ln(ln(A_t/A_∞)) = ln(k_{II}[Fe^{III}]$_t$/k_i) − $k_i t$; A_t and A_∞ are absorbances at time t and at the end of the cycle ($t = \infty$), respectively; [Fe^{III}]$_t$ is the total catalyst concentration. The inactivation rate constant k_i for **1a** at pH 11 and 25 °C, of (1.78 ± 0.05) × 10^{-3} s^{-1}, obtained in this work, is indeed significantly lower than that for the related **1d** of (13 ± 1) × 10^{-3} s^{-1}.[4] While the slightly larger **1a** rate constant k_{II} [(1.20 ± 0.03) × 10^5] lies within experimental error for **1d** [(1.0 ± 0.2) × 10^5 M^{-1} s^{-1}], the ratio k_{II}/k_i is 9.6 times greater for **1a** than for **1d** representing a pronounced catalytic advantage for the former.

Rate of H$_2$O$_2$ Activation (iii) and Operation pH (iv). The new data in Figure 1 indicate that the pH profile for the second order rate constant k_I for the reaction between an Fe^{III}−TAML and ^{t}BuOOH, which in aqueous solution affords various Fe^{IV} species[9] perhaps via an Fe^V-oxo species,[10] is shifted toward neutral pH for **1a** compared to the prototype **1b**. These bell-shaped graphs are quantifiable in terms of eq 1 which has been derived assuming the stoichiometric mechanism shown in Scheme 2 where the k_2 and k_3 pathways are kinetically indistinguishable.[6] A shift to pH ca. 10.5 from ca. 12 for the maximum rate of ^{t}BuOOH activation (both are
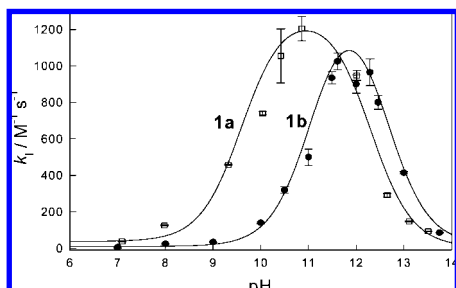
Figure 1. pH profiles for the rate constants k_I obtained by the stopped-flow technique for the reactions of **1b** (●) and **1a** (□) with ′BuOOH in 0.01 M phosphate at 25 °C. Solid lines are calculated using the best-fit values of k_1, k_2, k_4 (all in $M^{-1} s^{-1}$), pK_{a1}, and pK_{a2} of 37 ± 2, $(1.4 \pm 0.1) \times 10^3$, 20 ± 1, 9.7 ± 0.2, and 12.0 ± 0.4 for **1a**, and 10 ± 0.2, $(1.3 \pm 0.2) \times 10^3$, 15 ± 1, 10.8 ± 0.1, and 12.6 ± 0.2 for **1b**, respectively. The pK_{a2} values obtained here agree with that of 12.4 measured directly elsewhere.[11]

Scheme 2. The Mechanism of Reactions of **1** with Peroxides in Water That Accounts for the pH Profiles Such as in Figure 1
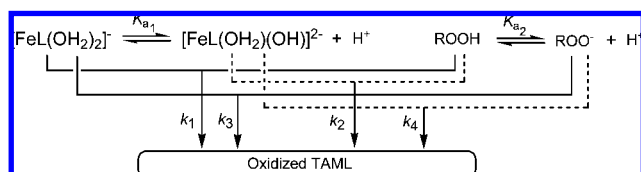
lower for H_2O_2) does indeed arise for **1a**, as anticipated from the decrease in pK_{a1} compared to **1b**. Therefore, the maximum rate for the **1a**-catalyzed oxidations by H_2O_2 would occur at pH 9−9.5.[6] The value of pK_{a1} for **1a** of 9.7 ± 0.2 was obtained by fitting the experimental ′BuOOH data to eq 1 (Figure 1), close to the spectrophotometrically determined value of 9.3 ± 0.5.[3] Although there is room for further improvement, this is the lowest pK_{a1} measured for an Fe^{III}−TAML activator signaling significant success in moving the greatest rate toward neutral pH. A LFER for Fe^{III}−TAMLs between the pK_{a1} values and the rate constants k_I (Figure 2S) exhibits a slope ≈ -1, showing that the Lewis acidity of iron(III) is key in determining each activator's acid−base properties and reactivity.

$$k_I = \frac{k_1[H^+]^2 + (k_2 K_{a_1} + k_3 K_{a_2})[H^+] + k_4 K_{a_1} K_{a_2}}{[H^+]^2 + (K_{a_1} + K_{a_2})[H^+] + K_{a_1} K_{a_2}} \quad (1)$$

DFT optimized structures of **1** agree well with results obtained by X-ray crystallography.[12] For **1a**, the DFT optimized structure does not significantly differ from other Fe^{III}−TAMLs. The four amide N atoms are almost planar (mean rms deviation ∼1.6°). The Fe-OH$_2$ bond distance is 2.14 Å (Figure 2A). There is a strong OH$_2$···F$_{tail}$ H-bond of 1.84 Å, found for other F-tailed **1**s. The Mulliken charge at iron in **1a** is higher than for **1e** and comparable to that of **1d**. Figure 2B shows that the charge on the Fe correlates with the key peroxidase-like reactivity (k_{II}) of **1** suggesting that this charge is a valuable design tool for Fe^{III}−TAMLs. The Fe-OH$_2$ bond distance is also related to the positive charge density at iron; the **1a** Fe-OH$_2$ distance [2.14 Å] is shorter than **1b**'s [2.23 Å], implying when peroxides bind a stronger RO(H)O−Fe bond forms for **1a** inducing a more acidic peroxide α-proton and favoring a more rapid O−O bond cleavage.
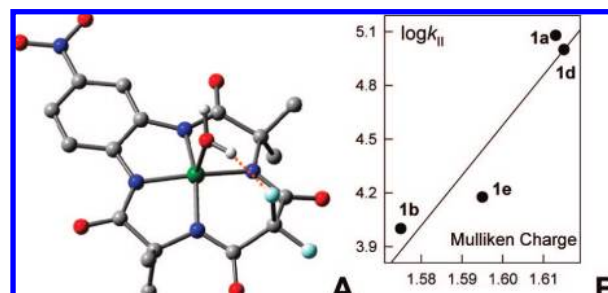
Figure 2. (A) DFT-optimized geometry of **1a** (B3LYP, 6-311G basis set, Gaussian 03 (release C.02). H atoms other than those of axial H$_2$O are not shown. The dotted line shows a strong H-bond. (B) The rate constants k_{II} for the Safranine O bleaching against the Mulliken charges at iron.[4]

In conclusion, **1a** has been designed on the basis of multiple kinetic parameters and the Mulliken charge at iron to deliver superior performance. It is the most medium and operationally stable, the most reactive with a pH of maximum activity closest to 7 among current Fe^{III}−TAMLs. However, **1a**'s fluorine is biochemically unfamiliar. Deployment for large-scale water treatment could lead to unacceptable buildup of environmentally mobile, persistent fluorinated degradation fragments with unknown environmental implications. With peroxidases at last functionally mimicked, precautionary challenges associated with finding alternatives to F-substituted tails that deliver exceptionally aggressive, halogen-free catalysts define the Fe^{III}−TAML design frontier.

Supporting Information Available: Experimental procedures and results, details of DFT calculations, Figures 1S and 2S. This material is available free of charge via Internet at http://pubs.acs.org.

References

(1) Collins, T. J. *Acc. Chem. Res.* **2002**, *35*, 782–790.
(2) Collins, T. J.; Walter, C. *Sci. Am.* **2006**, *294*, 83–88; 90.
(3) Ghosh, A.; Ryabov, A. D.; Mayer, S. M.; Horner, D. C.; Prasuhn, D. E., Jr.; Sen Gupta, S.; Vuocolo, L.; Culver, C.; Hendrich, M. P.; Rickard, C. E. F.; Norman, R. E.; Horwitz, C. P.; Collins, T. J. *J. Am. Chem. Soc.* **2003**, *125*, 12378–12378.
(4) Chanda, A.; Ryabov, A. D.; Mondal, S.; Alexandrova, L.; Ghosh, A.; Hangun-Balkir, Y.; Horwitz, C. P.; Collins, T. J. *Chem.—Eur. J.* **2006**, *12*, 9336–9345.
(5) Chahbane, N.; Popescu, D.-L.; Mitchell, D. A.; Chanda, A.; Lenoir, D.; Ryabov, A. D.; Schramm, K.-W.; Collins, T. J. *Green Chem.* **2007**, *9*, 49–57.
(6) Ghosh, A.; Mitchell, D. A.; Chanda, A.; Ryabov, A. D.; Popescu, D. L.; Upham, E.; Collins, G. J.; Collins, T. J. *J. Am. Chem. Soc* in press.
(7) Polshin, V.; Popescu, D.-L.; Fischer, A.; Chanda, A.; Horner, D. C.; Beach, E. S.; Henry, J.; Qian, Y.-L.; Horwitz, C. P.; Lente, G.; Fabian, I.; Münck, E.; Bominaar, E. L.; Ryabov, A. D.; Collins, T. J. *J. Am. Chem. Soc.* **2008**, *130*, 4497–4506.
(8) Patents: http://www.chem.cmu.edu/groups/Collins/awardpatpub/patents/index.html.
(9) Chanda, A.; Shan, X.; Chakrabarti, M.; Ellis, W.; Popescu, D.; Tiago de Oliveria, F.; Wang, D.; Que, L., Jr.; Collins, T. J.; Münck, E.; Bominaar, E. L. *Inorg. Chem.* **2008**, *47*, 3669–3678.
(10) Tiago de Oliveira, F.; Chanda, A.; Banerjee, D.; Shan, X.; Mondal, S.; Que, L., Jr.; Bominaar, E. L.; Münck, E.; Collins, T. J. *Science* **2007**, *315*, 835–838.
(11) Davies, G.; Garafalo, A. R. *Inorg. Chem.* **1976**, *15*, 1101–1106.
(12) Chanda, A.; Popescu, D.-L.; Tiago de Oliveira, F.; Bominaar, E. L.; Ryabov, A. D.; Münck, E.; Collins, T. J. *J. Inorg. Biochem.* **2006**, *100*, 606–619.

JA805099E